

Training trajectories, mini-batch losses and the curious role of the learning rate.

Mark Sandler Andrey Zhmoginov Max Vladymyrov
 Nolan Miller
 Google Research
 {sandler,azhmogin,mxv,namiller}@google.com

Abstract

Stochastic gradient descent plays a fundamental role in nearly all applications of deep learning. However its ability to converge to a global minimum remains shrouded in mystery. In this paper we propose to study the behavior of the loss function on fixed mini-batches along SGD trajectories. We show that the loss function on a fixed batch appears to be remarkably convex-like. In particular for ResNet the loss for any fixed mini-batch can be accurately modeled by a quadratic function and a very low loss value can be reached in just one step of gradient descent with sufficiently large learning rate. We propose a simple model that allows to analyze the relationship between the gradients of stochastic mini-batches and the full batch. Our analysis allows us to discover the equivalency between iterate aggregates and specific learning rate schedules. In particular, for Exponential Moving Average (EMA) and Stochastic Weight Averaging we show that our proposed model matches the observed training trajectories on ImageNet. Our theoretical model predicts that an even simpler averaging technique, averaging just two points a many steps apart, significantly improves accuracy compared to the baseline. We validated our findings on ImageNet and other datasets using ResNet architecture.

1 Introduction

Stochastic Gradient Descent (SGD; Robbins & Monro, 1951) played a fundamental role in the rise

and success of deep learning. Similarly, the learning rate, the multiplier controlling the magnitude of the weight update, is perhaps the most crucial hyper-parameter that controls the training trajectory (Goodfellow et al., 2016; Smith, 2015; Bengio, 2012; Smith, 2015). Despite the advances in stochastic optimization methods (Kingma & Ba, 2014) designed to reduce the need for tuning, and in particular dependence on learning rate, novel learning rate schedules such as cosine (Loshchilov & Hutter, 2016) and cyclical learning rate schedule (Smith, 2015) continue to be the subject of active research and are far from being rigorously understood. On the other hand, the impact of stochasticity of the optimization process caused by changing input mini-batches also known as "batch noise", (Ziyin et al., 2021) has been relatively poorly understood. In

Contributions In this paper we show that the loss as a function of learning rate of the training batch is dramatically different than that on the held-out batch, when measured on SGD trajectory. This connection to learning rate leads to a simple theoretical model describing observed results. We believe this connection of the learning rate to the loss as a function of held out and training match has been largely overlooked in the literature.

One practical result that we demonstrate that various popular averaging techniques have equivalent learning rate schedules. To the best of our knowledge such connection has not been observed in the literature. We demonstrate the equivalency in two

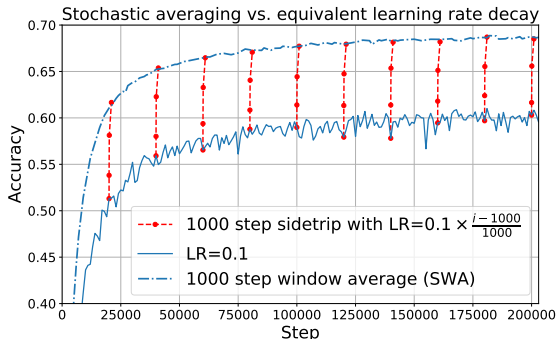


Figure 1: Weight averaging v.s. equivalent learning rate schedule. The dotted vertical red lines show the set of independent trajectories “sidetrips” with appropriate learning rate schedule that start at corresponding point in the main trajectory.

different scenarios: a simple scenario where we assume that the gradient for the same input changes little between steps, and the other where we show that this equivalency holds in the limit case of an arbitrary long trajectory. We demonstrate (e.g. Figure 1) that these results hold empirically for a general training of ImageNet (Russakovsky et al., 2015) using ResNet architecture (He et al., 2015).

We propose a simple model that captures these behaviors. The model we consider is similar to that of Mandt et al. (2017), but our analysis is noticeably simpler. We further show that our simple model is suitable for studying training trajectories with a spectrum of time scales ranging from fast to slow and corresponding to long trenches in the loss landscape. We show how model weights quickly converge towards a quasi-stationary distribution in some degrees of freedom, while slowly drifting towards the global minimum in others and derive the expression for the auto-correlation of the averaged trajectory as a function of the averaging kernel (Appendix A).

Using this model we develop a simple geometric explanation of why averaging improves the accuracy in the first place. We show that even on large datasets such as ImageNet and for deep architectures using the fixed learning rate the trajectory traverses an ellipsoid centered around the target minimum and the av-

eraging moves the trajectory to the inside of that ellipsoid. Further, we show that for two independently trained trajectories that share a common burn-in period the *distance* in parameter space along one trajectory to the final solution of another monotonically decreases as training progresses and asymptotically stabilizes at a fixed value. This suggests that most of the probability mass of the training outcomes is concentrated on a sphere-like volume.

Our final insight is the dramatic difference in the behavior of the loss function for the batch that it is being optimized v.s. a new (training) batch. We are not aware of any study in the literature that explores this difference. While this is reminiscent of the generalization gap, there is a crucial distinction: we analyze the loss on a different *training* batch, and not on a validation batch. To some degree our work also illuminates the approach of Amortized Proximal Optimization (Bae et al., 2022) that used the loss on the unseen batch referred as *Functional Space Discrepancy*, as a negative regularization force for learning rate selection. Curiously their motivation was to reduce the change of the loss on the unseen batch as a way to minimize the predictions on unseen data. However, as we demonstrate here, such type of adaptive schedule tries to apply asymptotically *largest* update, that prevents loss on unseen batches to *increase* and thus the training to diverge.

Interestingly, such difference in gradients and behavior of two training batches, also indicates that a simple intuition (Ziyin et al., 2021; Mandt et al., 2017; Sato & Nakagawa, 2014b) that stochastic gradient descent is an approximation to batch gradient could be misleading and thus should be used judiciously, despite it being unbiased estimate of the full gradient.

Paper organization The paper is organized as follows. In the next section we describe some of the ImageNet experiments that led us to our theoretical model described in section Section 4. In Section 5 we show some additional experiments on both real data and synthetic model that we introduced in Section 4. Finally in Section 6 we outline some of the open questions and future directions.

2 Related work

Averaging intermediate SGD iterates in the weight space can be traced back to Ruppert (1988). In more recent years it became a common tool for speeding up convergence (Kaddour, 2022) and improving accuracy (Izmailov et al., 2018). It was first directly analyzed in Polyak & Juditsky (1992) and has been studied in the literature since. For example in Mandt et al. (2017) the connection between SGD and Bayesian inference was established. In particular they demonstrated that SGD training that initialized within common zone of attraction can be seen as Markov chain with Gaussian stationary distribution for constant learning rate, which is related to our observation about trajectory stabilizing at a fixed distance from the global minimum. However in present work we mainly analyze the behavior of a single trajectory. This has immediate advantage that it allows us to reason about *finite* trajectory lengths, as well as the connection between learning rate schedules and averaging.

Another related line of inquiry is *Stochastic Weight Averaging* (SWA) by Izmailov et al. (2018), where a trajectory with cyclic learning rates and averaging every c steps is used as a way to improve accuracy. This in theory is slightly different from Ruppert-Polyak averaging, since not every point on the trajectory is averaged, however, many of the experiments presented in that paper use $c = 1$ and we suspect this difference is insignificant. In that work it was also observed that averaging between trajectory allows to move inside the surface, but no further discussion has followed. Additionally, the connection between SWA and generalization was further explored in He et al. (2019), where it was showed that averaging introduces bias towards flatter part of the basin and this results in better generalization. In contrast here our goal is to illuminate the mechanisms by which SWA changes the behavior of empirical loss in the context of *stochastic* (rather than full) gradient descent. Connecting current work and the generalization performance is an interesting open direction. The quadratic theoretical model we consider is reminiscent of that in Schaul et al. (2013), but our analysis is both simpler than former and more general than latter. We

note that analysis only applies to *stochastic* gradient descent. In case of full gradient descent there have been several recent works showing that quadratic approximation model might be too simplistic (Ma et al., 2022; Damian et al., 2022; Cohen et al., 2021).

Recent work on basins and local minima connectivity (Ainsworth et al., 2022; Benzing et al., 2022; Frankle et al., 2019) have demonstrated that there is a lot of apparent structure in the loss space, in particular it was shown that different initialization lead to different equivalence classes, which can then be mapped between each other using simple permutation of the neurons. That work is complementary to ours in that they show that there are simple ways of moving basins, while we concentrate on properties of a single basin.

3 Empirical observations

In this section our goal is to explore some of the properties of SGD that will lead us to the theoretical model of Section 4.

Experimental setup For all our experiments with non-synthetic data we use ResNet34 (He et al., 2015) architecture and ImageNet (Russakovsky et al., 2015). We use standard SGD with momentum 0.9, that produces good accuracy on ImageNet. Most of our experiments on real data involve starting with partially trained architectures, and running a separate *side-trip* with different learning rate characteristics and/or with a fixed *training* mini-batch to demonstrate certain behaviors. We also will use the notion of *held-out* mini-batch which is simply a *fixed* batch different from the training mini-batch. Throughout this section we will be referring to the training trajectory as the *main* trajectory to differentiate from side-trips.

Single step experiments We begin with a simple question: how does a loss landscape look for a single batch applied with a varying learning rate? Specifically, does the loss behave on that batch v.s. a separate held-out batch? In Figure 2 we plot the loss v.s. the learning rate when applied to a single step using

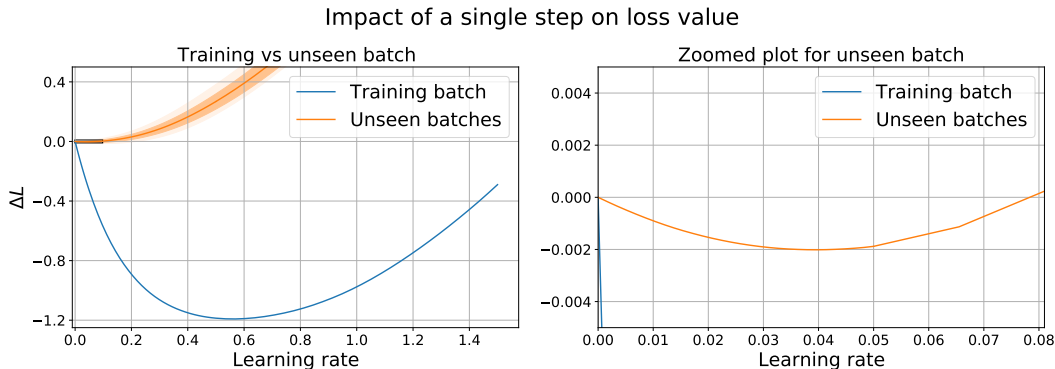


Figure 2: Loss as a function of a step size in a single step gradient descent in the middle of a trajectory. The step shown here is step 75 000 out of 100 000 run. The behavior is typical for other steps as well. The small rectangle on the left graph approximately shows the location of the zoomed-in right graph. The unseen batches is computed over 10 batches, with dark shade showing the standard deviation from the mean, while light shade shows the max/min values observed.

either the batch for which the direction was computed or a separate held-out batch. Here we used step 75K, out of 100K, and batch size 512, however very similar results hold elsewhere in the trajectory and for different batch sizes. See Appendix B.1 for details.

As can be seen from Figure 2 the loss for both curves is smooth and can be well approximated by a low-degree polynomial. More importantly, the loss on the training batch reaches loss value below the average loss of a fully trained model in a single step. Typical loss value for fully trained ImageNet is close to 1, while a single step starting from the loss value 1.8 results in a final loss of 0.5. The loss on the held-out batch behaves very differently: only sufficiently small learning rate leads to any improvement to the loss on the full distribution. Therefore any analytical model purporting to describe SGD trajectories should have this property. Remarkably this suggests that full gradient trajectory is not a good approximation of the SGD trajectory, if we want to understand the dynamics of learning rate selection.

Multi-step side-trip As we just observed, a single step along the training batch direction can bring the loss down to values considerably lower than the best average loss of a fully trained model. Naturally one can ask – does the loss basin for this specific batch

remains the same regardless of the starting point? In other words, if we apply gradient descent with a fixed batch at one point of the main trajectory, would it be the same minima basin as if started from different point of the main trajectory? Note: this question is different from the notion of the global basin connectivity explored in Frankle et al. (2019). Instead, we look at the behavior of the loss for a fixed mini-batch as we branch off different parts of the training trajectory. Following the analysis of Frankle et al. (2019) we use interpolation to check that we are in the same basin. In Figure 3 we show that the side-trip using the same fixed batch along the main training trajectory leads to the same basin. Remarkably, the held-out batch loss while increasing dramatically also stays in the same basin as the main trajectory.

4 Analytical model

In this section we propose a model describing the behavior of the high dimensional weight vector θ , as it moves along the SGD trajectory, in such a way that it can explaining the phenomena that we described in Section 3: the loss for the individual batches behaves like a low-degree polynomial and reaches remarkably low value in a single step. Thus we can use quadratic

Interpolation between two trajectories with fixed-batch starting at θ_t and $\theta_{t+10000}$

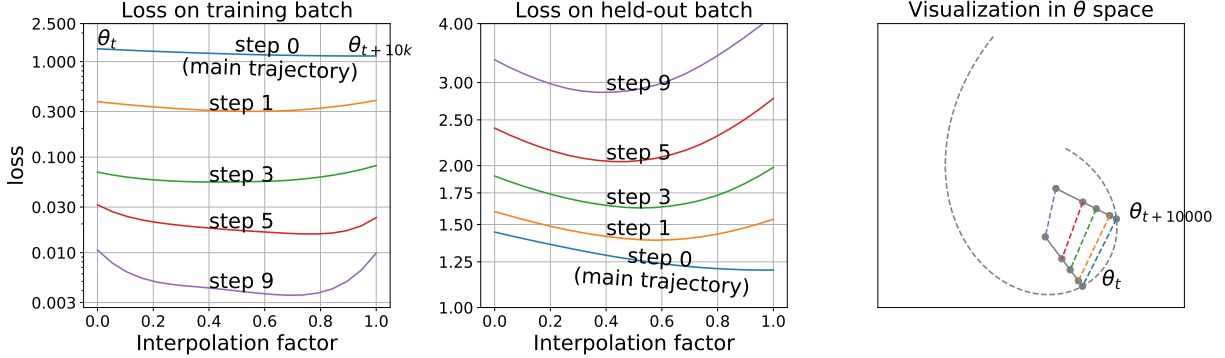


Figure 3: Loss for a fixed batch on the interpolation between two points of the original training trajectory. We use two points along the ImageNet training trajectory with $t = 75\,000$, and $t = 85\,000$. From each point we perform 9 steps of gradient descent on a fixed batch and measure the loss on interpolation between corresponding pairs of points of each trajectory. The left graph shows the loss on the training batch, and note how within just 3 steps it reaches nearly 0. The middle graph shows the loss on held out. At step 0 the training and held out batch loss profiles are very similar. Rightmost graph shows the visualization of the process.

function that models the loss function for individual samples:

$$L(\theta, x) = \|A_x \theta + c_x\|^2 / 2,$$

where A_x is a matrix and c_x is a vector describing the loss function for a random sample $x \sim D$. This model is similar to the one proposed in Schaul et al. (2013), however it analyzed only the special case of a constant and diagonal A_x , while we consider a general scenario. Following the mini-batch gradient where individual batches are sampled from some distribution we then will be moving in a direction whose expectation is $E_{x \sim D} \left[\frac{\partial L(\theta, x)}{\partial \theta} \right] = \frac{\partial E_{x \sim D} [L(\theta, x)]}{\partial \theta}$. Without loss of generality we will assume that $\frac{\partial E_{x \sim D} [L(0, x)]}{\partial \theta} = 0$.

The global loss over the sample distribution \mathcal{D} is

$$\begin{aligned} L(\theta) &= E_{x \sim \mathcal{D}} [L(\theta, x)] \\ &= \theta^T E_{x \sim \mathcal{D}} [A_x^T A_x] \theta + E_{x \sim \mathcal{D}} [c_x^T A_x] \theta + \\ &\quad + E_{x \sim \mathcal{D}} [c_x^T c_x] \\ &= \theta^T E_{x \sim \mathcal{D}} [A_x^T A_x] \theta + E_{x \sim \mathcal{D}} [c_x^T c_x] \end{aligned} \quad (1)$$

where we take expectation over all possible samples.

The last transition holds since we assumed that the loss function achieves minimum at 0, and thus A_x and c_x satisfy $E[A_x^T c_x] = 0$.

The stochastic gradient and the full gradient can then be written respectively as:

$$\frac{\partial L(\theta, x)}{\partial \theta} = A_x^T (A_x \theta + c_x). \quad (2)$$

$$\frac{\partial L(\theta)}{\partial \theta} = \frac{\partial E_{x \sim \mathcal{D}} [\|A_x \theta + c_x\|^2 / 2]}{\partial \theta} \quad (3)$$

$$= E_{x \sim \mathcal{D}} [A_x^T (A_x \theta + c_x)]. \quad (4)$$

Now we estimate how close we can get to 0 for a fixed learning rate. Note, even though the individual steps gradients can be assumed to be unbiased estimators of global loss gradient, there is generally no guarantee that trajectory will converge to a minimum. Instead we can show that the trajectory will be *traversing* an ellipsoid around the minimum.

Lemma 1 *If $E_{x \sim \mathcal{D}} [A_x^T A_x] = I$ the trajectory will stabilize at an ellipsoid of a fixed size proportional to the square root of the learning rate $\sqrt{\lambda}$.*

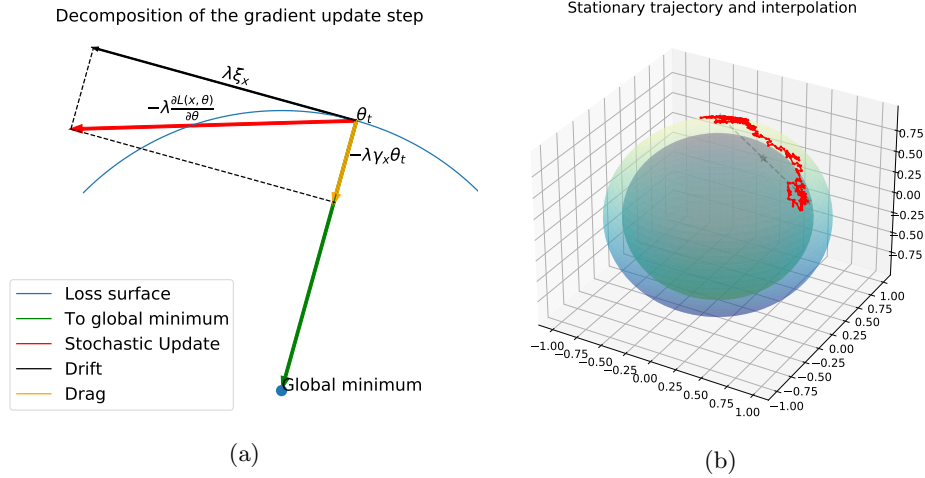


Figure 4: Stochastic gradient descent. Figure 4a shows how stochastic gradient direction decomposes into a drift and a drag component. The magnitude of the drag component changes as $\sqrt{\lambda}$, while the magnitude of the drift component is proportional to λ . Further, the drift component has a quadratic bias to increase loss, thus enabling us to pick learning rate that allows to reduce the loss. Figure 4b illustrates how stationary trajectory traverses the sphere of a fixed loss, while taking a midpoint enables to get *inside* the sphere. Best viewed in color.

Proof: Consider a fixed sample x at step t . Let $b_x := c_x^T A$.

$$\theta_{t+1} = \theta_t - \lambda A_x^T A_x \theta_t - \lambda b_x. \quad (5)$$

We would like to describe the behavior of $\|\theta_{t+1}\| - \|\theta_t\|$ as a function of λ . First, we observe that $\lambda \theta_t^T A_x^T A_x \theta_t \geq 0$, with equality achieved only when $A_x \theta_t = 0$. Thus, the second term in Equation (5) can be decomposed into a projection onto θ_t and its orthogonal component using the inner product with θ_t :

$$\lambda A_x^T A_x \theta_t = \lambda [\gamma_x \theta_t + \theta_{t, A_x}^\perp]$$

where $\gamma_x := \frac{\theta_t^T A_x^T A_x \theta_t}{\|\theta_t\|^2}$, and θ_{t, A_x}^\perp is a vector orthogonal to θ_t . Therefore the update Equation (5) can be rewritten as:

$$\theta_{t+1} = (1 - \lambda \gamma_x) \theta_t - \lambda [\theta_{t, A_x}^\perp + b_x] = (1 - \lambda \gamma_x) \theta_t - \lambda \xi_x \quad (6)$$

where

$$\xi_x := \theta_{t, A_x}^\perp + b_x. \quad (7)$$

The update to θ_t consists of two terms: (a) the component $-\lambda \gamma_x \theta_t$, whose magnitude depends on A_x that reduces norm of θ and (b) an orthogonal drifting term ξ_x . The term ξ_x also consists of two components: θ_{t, A_x}^\perp which is orthogonal to θ_t by construction, and $b_x = A_x^T c_x$ which we can assume to be orthogonal to θ_t since it is independent of the orientation of θ_t . Thus, ξ_x is orthogonal to θ_t and is determined by A_x, c_x and θ_t . These components are illustrated on Figure 4a. Most importantly the drift component ξ_x is approximately orthogonal to θ and its contribution to $\|\theta_{t+1}\|^2$ is quadratic in λ , while the drag component, has a linear contribution. Let us compute the change in norms given x :

$$\begin{aligned} \|\theta_{t+1}\|^2 - \|\theta_t\|^2 &= (1 - \lambda \gamma_x)^2 \|\theta_t\|^2 + \lambda^2 \|\xi_x\|^2 - \|\theta_t\|^2 \\ &= -\lambda \gamma_x (2 - \lambda \gamma_x) \|\theta_t\|^2 + \lambda^2 \|\xi_x\|^2, \end{aligned} \quad (8)$$

therefore the change in norm becomes zero when

$$\lambda = \lambda_x := \frac{2\gamma_x \|\theta_t\|^2}{\|\xi_x\|^2 + \gamma_x^2 \|\theta_t\|^2}. \quad (9)$$

Now we can estimate the *expected* change in norm for a fixed θ_t using Equation (8):

$$E_{x \sim \mathcal{D}} [\|\theta_{t+1}\|^2 - \|\theta_t\|^2 | \theta_t] = -2\lambda \|\theta_t\|^2 E_{x \sim \mathcal{D}} [\gamma_x | \theta_t] + \lambda^2 E_{x \sim \mathcal{D}} [\|\xi_x\|^2 + \gamma_x^2 \|\theta_t\|^2 | \theta_t]. \quad (10)$$

The expected change in norm becomes zero when

$$\lambda = 2\|\theta_t\|^2 \frac{E_{x \sim \mathcal{D}} [\gamma_x | \theta_t]}{E_{x \sim \mathcal{D}} [\|\xi_x\|^2] + \|\theta_t\|^2 E_{x \sim \mathcal{D}} [\gamma_x^2 | \theta_t]}, \quad (11)$$

or, equivalently, for fixed λ the norm has zero expected change

$$\begin{aligned} \|\theta_t\|^2 &= \frac{\lambda E_{x \sim \mathcal{D}} [\|\xi_x\|^2 | \theta_t]}{2E_{x \sim \mathcal{D}} [\gamma_x | \theta_t] - \lambda E_{x \sim \mathcal{D}} [\gamma_x^2 | \theta_t]} \\ &= \frac{\lambda E_{x \sim \mathcal{D}} [\|\xi_x\|^2 | \theta_t]}{2E_{x \sim \mathcal{D}} [\gamma_x | \theta_t]} + O(\lambda^2). \end{aligned} \quad (12)$$

For the special case when $E_{x \sim \mathcal{D}} [A_x^T A_x] = I$, we have $E_{x \sim \mathcal{D}} [\gamma_x | \theta_t] = I$, and since A_x is independent of θ_t we can assume that θ_{t, A_x}^\perp is orthogonal to b_x and its magnitude is independent of θ_t , therefore $E_{x \sim \mathcal{D}} [\|\xi\|^2 | \theta] \approx E_{x \sim \mathcal{D}} [\|\xi\|^2]$ and thus

$$\|\theta\| = \sqrt{E_{x \sim \mathcal{D}} [\|\xi\|^2]} \sqrt{\lambda/2} = \|c\| \sqrt{\lambda/2}. \quad (13)$$

■

For a fixed learning rate we can expect the distance to the global minimum to stabilize at a value proportional to $\sqrt{\lambda}$ and described by Equation (13).

This model turns out to be very similar to additive batch-noise model of Wu et al. (2019) and Schaul et al. (2013), however instead of introducing it, we arrive to it from an empirical assumption that each batch optimizes its own loss function. Despite its simplicity it appears to capture well many of the phenomena of large deep neural networks training.

An alternative derivation of the result above is based on Fokker-Planck equation for describing the evolution of the state density (Sato & Nakagawa, 2014a; Li et al., 2017; Chaudhari & Soatto, 2018) and showing that the stationary solution of this equation is a Gaussian distribution (for which the samples are concentrated on a spherical shell). While in general this scaling factor is opaque, there are several special cases allowing for further simplification of the equation.

Weight averaging: effect on the stationary distribution. As we saw earlier, for a fixed learning rate the solution trajectory stabilizes an ellipsoid whose size is proportional to $\sqrt{\lambda}$, while traversing it indefinitely. If we let it continue sufficiently long we end up with two solutions θ_1 and θ_2 that are samples on the same sphere. Therefore the average $\theta = (\theta_1 + \theta_2)/2$ has norm $\|\theta\| = \|\theta\|/\sqrt{2}$. Thus averaging two solutions with a higher learning rate λ gives us practically identical solution as if following the trajectory from θ_1 to θ_2 , but with the learning rate $\lambda/2$. Geometrically, the interpolation between two points on a random trajectory results in a point inside the sphere (Figure 4b), which translates to a lower loss. Remarkably similar effects are also observed for ImageNet as we show in Figure 5. In Appendix A we generalise this result to an arbitrary averaging kernel.

We note that previous interpretations proposed in Kingma & Ba (2014) suggest that weight averaging works by “smoothing” the model. Instead, we show that there is a natural geometric interpretation that arises from the basic properties of stochastic gradient descent. Similar intuition can also be applied to stochastic weight averaging (SWA; Izmailov et al., 2018) and exponential moving averaging (EMA; Kingma & Ba, 2014).

Weight averaging: equivalence to the reduced learning rate along the trajectory. As we saw above, aggregation is equivalent to a specific learning schedule in the stationary regime. Here we consider another angle: we show that a similar result also holds when we look at window sizes, where we can assume that gradient on a fixed batch doesn’t change much along the trajectory. We formalize this result in the lemma below.

Lemma 2 (for proof see Appendix A) *If gradient of the loss with respect to a fixed batch is approximately constant, then for SWA with cycle of length $c = 1$, two-point averaging and EMA, the equivalent learning schedule is described in Table 1.*

Note that under our simplifying assumption of matching gradients, we have shown a much stronger result: not only losses match, but the actual trajectories match. In the actual training, as can be seen

Averaging method	Equivalent learning rate for last k steps
Stochastic Weight Averaging (Izmailov et al., 2018), window size k , cycle $c = 1$	$\lambda(i) \frac{k+1-i}{k}$
Two point average k step apart	$\lambda(i)/2$
Exponential Moving Average (decay δ)	$\lambda(i)(1 - (1 - \delta)^{k-i})$, where $(k \gg 1/\delta)$

Table 1: Equivalent learning rate schedules for different averaging methods. Here i denotes the current step of SGD trajectory and $\lambda(i)$ is a learning rate pre-aggregation. Even though EMA is computed over the entire trajectory, the contributions of points beyond $1/\delta$ decay exponentially, thus the equivalent schedule only need to be applied to the last $k \gg \frac{1}{\delta}$.

in Figure 7 the gradients, while staying fairly aligned, do exhibit some amount of divergence. Further the divergence in θ space is also significant (though much less than if batches were sampled independently). Despite that, we can see from Figure 5 that *loss* exhibit remarkable match between different averaging schemas and learning rate schedules. We conjecture that the requirements of this lemma can be relaxed in favor of loss match, where instead of matching the full trajectory, the different methods reach different points on the loss surface.

To recap, in our model we have shown that *both* stationary regime and early in the trajectory the weight aggregation has equivalent learning schedules. It remains a subject of future work to bridge the theory to include the *entire* trajectory, as appears to be the case for real deep neural networks.

5 Experiments

In this section we describe our additional experiments. Following our setup from Section 3, we experiment with ImageNet, but also include results from Cifar10 and Cifar100 (Krizhevsky, 2009). For all datasets we use identical setup with ResNet-34, and use SGD with momentum 0.9.

Different aggregation and learning rate schedule on ImageNet and CIFAR datasets In this experiment we show that learning rate schedules described in Table 1 match stochastic averaging on several large datasets. On Figure 5 we show our results

for the ImageNet. On Figure 5 we show validation accuracy, however similar results also hold for training splits as well for the actual losses, as we show in supplementary materials Appendix B.2. Additionally we include the results on Cifar10 and Cifar100 in the supplementary materials Figure 10.

On Figure 6 we show how the solution for two-point averaging diverges from the equivalent learning rate schedule. As can be seen, the training loss matches our estimate fairly close, while arriving at two distinct solutions. Even though the average point is significantly apart, in relative terms the two solutions are much closer than two independently trained solution with identical learning rate.

Gradient alignment and divergence of trajectories As we recall from Lemma 2, we relied on the gradients for a fixed batch essentially unchanging as we move along the trajectory. On Figure 7 we show that gradients on the fixed batch b indeed change very little. We consider two *side-trips*, using standard sequence of mini-batches, but we measure the gradient on a *fixed* mini-batch and compare its direction with the gradient at the initial step. As can be seen, the gradient norm changed less than 5%, while *cos* stayed generally above 0.5. For high dimensional space this means that the gradient on a fixed batch stays within a very narrow cone *throughout* the trajectory. Remarkably, the angle between two parallel points of two trajectories (green curve) is even closer aligned than the gradient between the end-point and the start point.

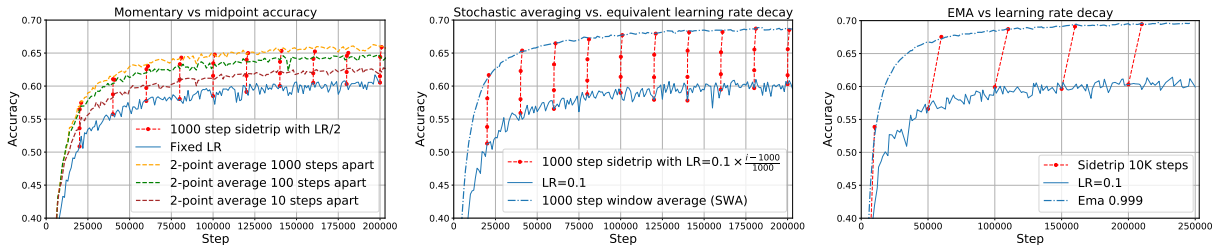


Figure 5: Comparing learning rate schedule with aggregation. The dotted vertical red lines show the set of independent trajectories “side-trips” with appropriate learning rate schedule that start at corresponding point in the main trajectory. For midpoint and average, the red circles at midpoint show the accuracy at 1, 10, 100 and 1000 steps. For EMA the side-trips are 3000 steps. The alternating dash/dot show the running averages of the main trajectory (solid line, bottom).

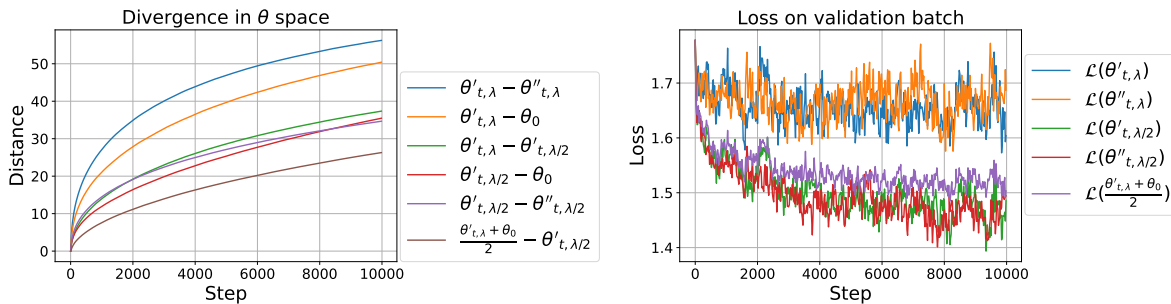


Figure 6: Evolution of L_2 distances divergence in weight space, the starting point θ_0 was selected at 75K, with the starting learning rate at $\lambda = 0.05$ and $\lambda/2$. θ' and θ'' correspond to two different trajectories using differently sampled mini-batches. Note how the loss of the average point of the trajectory with learning rate λ tracks the trajectory with $\lambda/2$.

For reference we also include the angle between two *independent* batches – as one can see those gradients are typically almost perfectly orthogonal. All this suggests that we can generally expect the requirements of lemma Figure 7 to hold even on large datasets.

Basins of attraction It has been known that multiple trajectories sharing initial segment end up in the attraction basin as measured by the absence of the loss barrier (Frankle et al., 2019). Here we show that in addition to being part of the same basin, the final point of one trajectory and an independent trajectory re-trained using different sequence of mini-batches monotonically decreases until saturates at some con-

stant level. On Section 5 we show how this distance changes for one such trajectory. This provides further evidence that independent trajectories land on a sphere around some fixed minimum.

5.1 Synthetic model experiments

Fast and slow convergence We have previously shown that the effect of weight averaging can be simulated approximately by using a properly chosen learning rate schedule. However, in practice, it is often advantageous to use fixed learning rate throughout training, especially if the new data is constantly arriving and the model needs to be trained continuously. In this case, the weight averaging can improve

Divergence of gradients for linearly decaying schedule

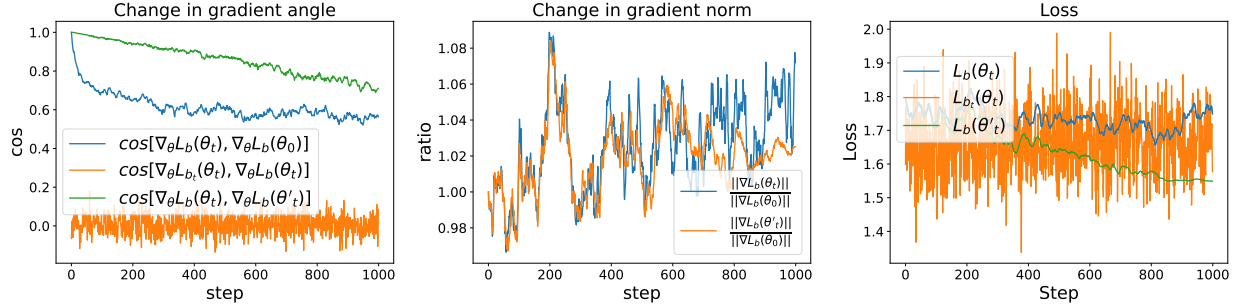


Figure 7: Evolution of L_2 gradient divergence, the starting point θ_0 was selected at 75K for different LR schedules. We compare fixed batch b and training batch b_t . For fixed batch the direction of the gradient changes very slowly over 1000 steps (blue curve), while for different batches (orange curve) all nearly orthogonal even at the same step. The top most (green curve) on the left chart is the cos of the angle between two gradients at trajectory θ_t - fixed learning rate of 0.05, and θ'_t - the linearly decaying learning rate $\lambda = 0.05 \frac{1000-i}{1000}$. The middle graph shows the change in gradient norm between different schedules. The rightmost graph, (orange curve) shows the losses for training batch, while the green curve and blue curve show the loss of a fixed batch b for constant and linearly decaying schedule respectively. Note that while green and blue curves maintain good gradient alignment, despite green curve exhibits significant loss change. Best viewed in color.

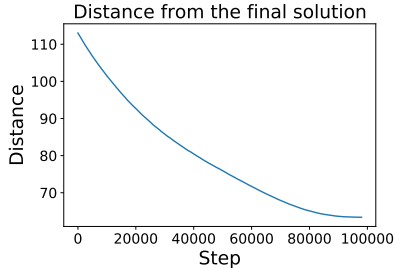


Figure 8: Distance between intermediate weights θ_t and an independently trained alternative solution θ'

model performance, while still allowing us to train the model with a large learning rate guaranteeing fast convergence.

The beneficial effect of weight averaging is particularly pronounced in situations where training dynamics is characterized by a wide spectrum of time scales, which is typical in practical scenarios (Ghorbani et al., 2019). This rich spectrum of timescales man-

ifests itself as the existence of elongated “trenches” in the loss landscape and long tails characteristic for the evolution of the loss during training.

Since weight averaging is generally sensitive to the time scale of the underlying weight evolution, one can expect it to have different effects on “slow” and “fast” degrees of freedom. As discussed in Appendix A in more detail, weight averaging will have little effect on the slow dynamics, but is expected to reduce the size of the stationary distribution for fast degrees of freedom and reduce the corresponding contribution to the loss as if the learning rate was in fact smaller. Notice that using smaller learning rate without weight averaging would have a disadvantage of slowing down the convergence in slow coordinates and thus using large learning rate with weight averaging is expected to help us improve model performance without sacrificing the convergence speed.

We illustrate this intuition by solving equation 5 for $b_x \sim \mathcal{N}(0, \mathbb{1})$ and a diagonal $\langle A_x^T A_x \rangle$ with values 1 and 0.015 for the fast and slow degrees of freedom correspondingly. The evolution of the loss function

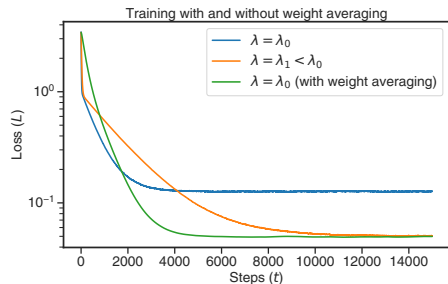


Figure 9: Loss dynamics in a system governed by with “fast” ($\Omega_{ii} = 1$) and “slow” ($\Omega_{ii} = 0.015$) degrees of freedom. Larger ($\lambda_0 = 5 \cdot 10^{-2}$) and smaller ($\lambda_1 = 2 \cdot 10^{-2}$) learning rates v.s. EMA;

in this system is shown in Figure 9 for two different learning rates: (a) $\lambda_0 = 5 \cdot 10^{-2}$ and (b) $\lambda_1 = 2 \cdot 10^{-2}$. Experiments with $\lambda = \lambda_0$ are conducted both with and without the exponential moving weight averaging (with a decay rate of 450 steps). Figure 9 illustrates that there are indeed two time scales in $L(t)$, fast and slow, and that weight averaging can dramatically reduce the stationary loss L without sacrificing the speed of convergence, unlike when training with the smaller learning rate $\lambda = \lambda_1$. Also, as shown in Figure 11b, in the appendix, weight averaging has a much larger effect on the fast degrees of freedom, significantly reducing corresponding contributions to the overall loss, while having only a mild effect on slow coordinates.

6 Open question and conclusions

We explored some remarkable properties of the learning rate in stochastic gradient descent, and demonstrated the novel connection between iterate averaging and learning rate schedules. We showed that this connection can be observed both in simple theoretical models and in large-scale training on multiple datasets. We hope that this work paves the way to further understanding on the role of the learning rate in training. One direction that we see is developing more general models that would allow to study other

phenomena commonly observed during training, such as overfitting and trajectory-dependent learning rate.

References

- Samuel K. Ainsworth, Jonathan Hayase, and Sidhartha Srinivasa. Git re-basin: Merging models modulo permutation symmetries, 2022. URL <https://arxiv.org/abs/2209.04836>.
- Juhan Bae, Paul Vicol, Jeff Z HaoChen, and Roger Grosse. Amortized proximal optimization, February 2022. URL <http://arxiv.org/abs/2203.00089>.
- Yoshua Bengio. Practical recommendations for gradient-based training of deep architectures. *arXiv*, June 2012. URL <http://arxiv.org/abs/1206.5533>.
- Frederik Benzing, Simon Schug, Robert Meier, Johannes von Oswald, Yassir Akram, Nicolas Zuchet, Laurence Aitchison, and Angelika Steger. Random initialisations performing above chance and how to find them. *arXiv*, September 2022. URL <http://arxiv.org/abs/2209.07509>.
- Pratik Chaudhari and Stefano Soatto. Stochastic gradient descent performs variational inference, converges to limit cycles for deep networks. In *6th International Conference on Learning Representations, ICLR 2018, Vancouver, BC, Canada, April 30 - May 3, 2018, Conference Track Proceedings*, 2018.
- Jeremy M. Cohen, Simran Kaur, Yuanzhi Li, J. Zico Kolter, and Ameet Talwalkar. Gradient descent on neural networks typically occurs at the edge of stability. *CoRR*, abs/2103.00065, 2021. URL <https://arxiv.org/abs/2103.00065>.
- Alex Damian, Eshaan Nichani, and Jason D Lee. Self-Stabilization: The implicit bias of gradient descent at the edge of stability. *arXiv*, September 2022. URL <http://arxiv.org/abs/2209.15594>.
- Jonathan Frankle, Gintare Karolina Dziugaite, Daniel M. Roy, and Michael Carbin. Linear mode connectivity and the lottery ticket hypothesis. *CoRR*, abs/1912.05671, 2019. URL <http://arxiv.org/abs/1912.05671>.
- Behrooz Ghorbani, Shankar Krishnan, and Ying Xiao. An investigation into neural net optimization via hessian eigenvalue density. In Kamalika Chaudhuri and Ruslan Salakhutdinov (eds.), *Proceedings of the 36th International Conference on Machine Learning, ICML 2019, 9-15 June 2019, Long Beach, California, USA*, volume 97 of *Proceedings of Machine Learning Research*, pp. 2232–2241. PMLR, 2019.
- Ian Goodfellow, Yoshua Bengio, Aaron Courville, and Yoshua Bengio. *Deep learning*, volume 1. MIT Press, 2016.
- Haowei He, Gao Huang, and Yang Yuan. Asymmetric valleys: Beyond sharp and flat local minima. *CoRR*, February 2019. URL <http://arxiv.org/abs/1902.00744>.
- Kaiming He, Xiangyu Zhang, Shaoqing Ren, and Jian Sun. Deep residual learning for image recognition. *arXiv*, December 2015. URL <http://arxiv.org/abs/1512.03385>.
- Pavel Izmailov, Dmitrii Podoprikin, Timur Garipov, Dmitry Vetrov, and Andrew Gordon Wilson. Averaging weights leads to wider optima and better generalization. *arXiv*, March 2018. URL <http://arxiv.org/abs/1803.05407>.
- Jean Kaddour. Stop wasting my time! saving days of imagenet and bert training with latest weight averaging. *CoRR*, 2022. URL <https://arxiv.org/abs/2209.14981>.
- Diederik Kingma and Jimmy Ba. Adam: A method for stochastic optimization. *arXiv*, 2014.
- Alex Krizhevsky. Learning multiple layers of features from tiny images. Technical report, U. Toronto, 2009. URL <https://www.cs.toronto.edu/~kriz/learning-features-2009-TR.pdf>.
- Qianxiao Li, Cheng Tai, and Weinan E. Stochastic modified equations and adaptive stochastic gradient algorithms. In Doina Precup and Yee Whye Teh (eds.), *Proceedings of the 34th International Conference on Machine Learning, ICML 2017*,

- Sydney, NSW, Australia, 6-11 August 2017, volume 70 of *Proceedings of Machine Learning Research*, pp. 2101–2110. PMLR, 2017.
- Ilya Loshchilov and Frank Hutter. SGDR: Stochastic gradient descent with warm restarts. *coRR*, August 2016. URL <http://arxiv.org/abs/1608.03983>.
- Chao Ma, Daniel Kunin, Lei Wu, and Lexing Ying. Beyond the quadratic approximation: the multi-scale structure of neural network loss landscapes. *coRR*, April 2022. URL <http://arxiv.org/abs/2204.11326>.
- Stephan Mandt, Matthew D Hoffman, and David M Blei. Stochastic gradient descent as approximate bayesian inference. *J. of ML Research*, pp. 1–35, April 2017. URL <http://arxiv.org/abs/1704.04289>.
- B T Polyak and A B Juditsky. Acceleration of stochastic approximation by averaging. *SIAM J. Control Optim.*, 30(4):838–855, July 1992. URL <https://doi.org/10.1137/0330046>.
- Herbert Robbins and Sutton Monro. A Stochastic Approximation Method. *The Annals of Mathematical Statistics*, 22(3):400 – 407, 1951. doi: 10.1214/aoms/1177729586. URL <https://doi.org/10.1214/aoms/1177729586>.
- David Ruppert. Efficient estimations from a slowly convergent robbins-monro process. Technical report, Cornell University, 02 1988.
- Olga Russakovsky, Jia Deng, Hao Su, Jonathan Krause, Sanjeev Satheesh, Sean Ma, Zhiheng Huang, Andrej Karpathy, Aditya Khosla, Michael Bernstein, Alexander C. Berg, and Li Fei-Fei. Imagenet large scale visual recognition challenge. *Int. J. Comput. Vision*, 115(3):211–252, December 2015. ISSN 0920-5691. doi: 10.1007/s11263-015-0816-y. URL <http://dx.doi.org/10.1007/s11263-015-0816-y>.
- Issei Sato and Hiroshi Nakagawa. Approximation analysis of stochastic gradient langevin dynamics by using fokker-planck equation and ito process. In *Proceedings of the 31th International Conference on Machine Learning, ICML 2014, Beijing, China, 21-26 June 2014*, volume 32 of *JMLR Workshop and Conference Proceedings*, pp. 982–990. JMLR.org, 2014a.
- Issei Sato and Hiroshi Nakagawa. Approximation analysis of stochastic gradient langevin dynamics by using Fokker-Planck equation and ito process. *Proceedings of Machine Learning Research*, 32(2):982–990, 2014b. URL <https://proceedings.mlr.press/v32/satoa14.html>.
- Tom Schaul, Sixin Zhang, and Yann LeCun. No more pesky learning rates. In *International conference on machine learning*, pp. 343–351. PMLR, 2013.
- Leslie N Smith. Cyclical learning rates for training neural networks. *arXiv*, June 2015. URL <http://arxiv.org/abs/1506.01186>.
- Jingfeng Wu, Wenqing Hu, Haoyi Xiong, Jun Huan, Vladimir Braverman, and Zhanxing Zhu. On the noisy gradient descent that generalizes as SGD. *arXiv*, June 2019. URL <http://arxiv.org/abs/1906.07405>.
- Liu Ziyin, Kangqiao Liu, Takashi Mori, and Masahito Ueda. Strength of minibatch noise in SGD. *arXiv*, February 2021. URL <https://openreview.net/pdf?id=uorVGbWV5sw>.

Supplementary materials for “Training trajectories, aggregation and the curious role of the learning rate”.

A Weight Averaging

In this section, we consider the evolution of θ governed by

$$\theta_{t+1} = \theta_t - \lambda A \theta_t - \lambda \tilde{b}_{\mathbb{B}}, \quad (14)$$

a simplified version of the finite-batch version of equation 5:

$$\theta_{t+1} = \theta_t - \frac{\lambda}{|\mathbb{B}|} \sum_{x \in \mathbb{B}} A_x^T A_x \theta_t - \frac{\lambda}{|\mathbb{B}|} \sum_{x \in \mathbb{B}} b_x,$$

where \mathbb{B} is a batch of samples, $A = \langle A_x^T A_x \rangle$ is a matrix and $\tilde{b}_{\mathbb{B}} \sim \mathcal{N}(0, C)$ is a multivariate normal random variable with covariance $C = \mathbb{Q}\mathbb{Q}^\top$.

Here, we first show how equation 14 can be reduced even further by using a coordinate transformation that whitens the batch noise. We then consider a moving average of the training trajectory, derive a simple equation governing it and characterize the resulting converged steady-state distribution.

A.1 Simplifying gradient descent equation

Stochastic gradient descent trajectories following equation 14 depend on both A and C matrices. Performing a change of coordinates $\theta_t = \mathbb{Q}u_t$, we can remove the dependence on one of the matrices if \mathbb{Q} is an invertible matrix such that $\mathbb{Q}\mathbb{Q}^\top = C$. Indeed, noticing that $\tilde{b}_{\mathbb{B}}$ can be represented as $-\mathbb{Q}\xi_{\mathbb{B}}$ with $\xi_{\mathbb{B}} \sim \mathcal{N}(0, 1)$, we obtain:

$$\mathbb{Q}u_{t+1} = \mathbb{Q}u_t - \lambda A \mathbb{Q}u_t + \lambda \mathbb{Q}\xi_{\mathbb{B}},$$

and finally get a simpler description of the stochastic gradient descent trajectory:

$$u_{t+1} = (\mathbb{I} - \lambda\Omega)u_t + \lambda\xi_t, \quad (15)$$

where our new equation depends on only one matrix $\Omega := \mathbb{Q}^{-1}A\mathbb{Q}$.

The solution of equation 15 can be obtained recursively and reads:

$$u_{t+1} = (\mathbb{I} - \lambda\Omega)^{t+1-\tau} u_\tau + \lambda \sum_{t'=\tau}^t (\mathbb{I} - \lambda\Omega)^{t-t'} \xi_{t'}. \quad (16)$$

A.2 Moving average of the SGD trajectory

In Section 4, we presented a simple intuitive explanation of the fact that the two-point average evolves similarly to an ordinary SGD trajectory with an effective learning rate of $\hat{\lambda} = \lambda/2$. Here we prove a more general result for an arbitrary averaging procedure.

Consider a training trajectory u_t solving equation 15 and let $\hat{u}_t \equiv \sum_{k=0}^{\infty} \mu_k u_{t-k}$ be some average of the training trajectory with the real averaging kernel $\{\mu_k \in \mathbb{R} | k \in 0, \dots, \infty\}$. It is easy to see that \hat{u}_t satisfies the following equation:

$$\hat{u}_{t+1} = (\mathbf{I} - \lambda\Omega)\hat{u}_t + \lambda \sum_{k=0}^{\infty} \mu_k \xi_{t-k}. \quad (17)$$

Introducing $\nu_t \equiv \sum_{k=0}^{\infty} \mu_k \xi_{t-k}$, we see that this random process is characterized by $\langle \nu_t \rangle = 0$ and an auto-correlation $C_{t,\delta} \equiv \langle \nu_t \nu_{t+\delta} \rangle = \sum_{k=0}^{\infty} \mu_k \mu_{k+\delta}$ independent of time t , where the averaging is performed over different realizations of the batch noise ξ .

The solution of equation 17 can be obtained by analogy with how solution 16 was obtained for equation 15:

$$\hat{u}_t = \Gamma^t \hat{u}_0 + \lambda \sum_{\tau=1}^t \Gamma^{t-\tau} \nu_{\tau},$$

where we introduce $\Gamma \equiv \mathbf{I} - \lambda\Omega$. Choosing $t = T$ for some sufficiently large T and assuming that all eigenvalues κ_k of Γ are characterized by $0 < \kappa_k < 1$, the first term ends up being exponentially small $\sim \exp(-\kappa_{\max} T)$ and

$$\hat{u}_T \approx \lambda \sum_{\tau=0}^{T-1} \Gamma^{\tau} \hat{\nu}_{\tau},$$

where $\hat{\nu}_{\tau} \equiv \nu_{T-\tau}$.

Now let us look at the distribution $p(\hat{u}_T)$ for a fixed time T and different realizations of ν . It is easy to see that $\langle \hat{u}_T \rangle = 0$ since $\langle \hat{\nu}_{\tau} \rangle = 0$ for each τ . Furthermore,

$$\langle \hat{u}_T \hat{u}_T \rangle = \lambda^2 \left\langle \sum_{\tau, \tau'=0}^{T-1} \Gamma^{\tau+\tau'} \hat{\nu}_{\tau} \hat{\nu}_{\tau'} \right\rangle = \lambda^2 \sum_{\tau, \tau'=0}^{T-1} \Gamma^{\tau+\tau'} \langle \hat{\nu}_{\tau} \hat{\nu}_{\tau'} \rangle.$$

Notice that here we average over different realizations of ν_t and assume homogeneity of ν_t in time since $C_{t,t'-t}$ is independent of t and only depends on the difference $t' - t$. Assuming that T is sufficiently large for both $\kappa_{\max} T \gg 1$ and $C_{t>T} \ll C_0$ to hold, we can approximate (changing the integration bounds where $\Gamma^{\tau+\tau'} C_{\delta}$ is vanishingly small):

$$\langle \hat{u}_T \hat{u}_T \rangle \approx \lambda^2 \left(\sum_{\tau=0}^{T-1} \Gamma^{2\tau} C_0 + 2 \sum_{\delta=1}^{T-1} \sum_{\tau=0}^{T-1} \Gamma^{2\tau+\delta} C_{\delta} \right).$$

Here the coefficient of 2 emerges because $C_{\delta} = -C_{\delta}$ for $\delta > 0$. This can also be rewritten as (replacing T with $T+1$):

$$\langle \hat{u}_{T+1} \hat{u}_{T+1} \rangle \approx \lambda^2 X_T \left(C_0 + 2 \sum_{\delta=1}^T C_{\delta} \Gamma^{\delta} \right), \quad (18)$$

where $X_T \equiv \sum_{\tau=0}^T \Gamma^{2\tau}$.

Now let us look at the limit of $T \rightarrow \infty$, assuming for simplicity that C_δ is bounded as $\delta \rightarrow \infty$ and assuming that the eigenvalues of $\Gamma = \mathbf{I} - \lambda\Omega$ are all smaller than 1. The expression for X_∞ can be simplified by relating it to Taylor series for $1/(1-x)$, specifically notice that:

$$(\mathbf{I} - \Gamma^2)X_\infty = (\mathbf{I} - \Gamma^2) \sum_{\tau=0}^{\infty} \Gamma^{2\tau} = \sum_{\tau=0}^{\infty} \Gamma^{2\tau} - \sum_{\tau=1}^{\infty} \Gamma^{2\tau} = \mathbf{I}$$

and therefore $X_\infty = (\mathbf{I} - \Gamma^2)^{-1}$. We can then approximate equation 18 as follows:

$$F \equiv \lim_{T \rightarrow \infty} \langle \hat{u}_{T+1} \hat{u}_{T+1} \rangle \approx \lambda^2 (\mathbf{I} - \Gamma^2)^{-1} \left(C_0 + 2 \sum_{\delta=1}^{\infty} C_\delta \Gamma^\delta \right),$$

or recalling that $\Gamma = \mathbf{I} - \lambda\Omega$:

$$F \approx \lambda(2\Omega - \lambda\Omega^2)^{-1} \left(C_0 + 2 \sum_{\delta=1}^{\infty} C_\delta \Gamma^\delta \right). \quad (19)$$

This final expression for F connects the covariance of the stationary distribution in the weight space to the autocorrelation of the averaging kernel μ_t . One important conclusion is that since $\mathbf{I} - \lambda\Omega$ is contracting (assuming Ω is positive-definite), the long tail of C_δ can be effectively cancelled by $(\mathbf{I} - \lambda\Omega)^\delta$. In other words, if the characteristic averaging time exceeds $1/\kappa$, where κ is the eigenvalue of $\mathbf{I} - \lambda\Omega$, then the corresponding width of the stationary distribution will be inhibited by weight averaging.

A.3 Two-point average

The final expression 19 can then be applied to an arbitrary averaging procedure. For example, the following result generalizes the geometric derivation for the two-point average to an arbitrary¹ learning rate λ and the distance Δ between steps.

Since we define the averaging procedure via $\mu_0 = 1/2$ and $\mu_\Delta = 1/2$ (and $\mu_k = 0$ otherwise), we obtain $C_0 = 1/2$ and $C_\Delta = 1/4$. Substituting this expression into equation 19, we obtain:

$$F_\Delta \equiv \lim_{T \rightarrow \infty} \langle \hat{u}_T \hat{u}_T \rangle \approx S_\lambda \frac{\mathbf{I} + (\mathbf{I} - \lambda\Omega)^\Delta}{2},$$

where $S_\lambda \equiv \lambda(2\Omega - \lambda\Omega^2)^{-1}$. This expression can also be interpreted as:

$$\hat{\lambda} = \lambda \frac{1 + (1 - \lambda\kappa)^\Delta}{2}, \quad (20)$$

where $\hat{\lambda}$ is the effective learning rate for a degree of freedom corresponding to an eigenvector of Ω with an eigenvalue of κ . This expression generalizes our previous observation that $\hat{\lambda} \approx \lambda$ for sufficiently small $\Delta \sim 1$ and $\hat{\lambda} \approx \lambda/2$ for $\Delta \gg 1$ when $(1 - \lambda\kappa)^\Delta \approx 0$.

¹ λ still needs to be sufficiently small for system dynamics to not diverge

A.4 Multi-point average

Now let us study weight averaging over n points separated by Δ steps each, i.e., $\hat{u}_t = n^{-1}(u_t + u_{t-\Delta} + u_{t-2\Delta} + \dots + u_{t-(n-1)\Delta})$. Since this corresponds to $\mu_{k\Delta} = 1/n$ for $k = 0, \dots, n-1$, we obtain:

$$C_{k\Delta} = \sum_{\tau=0}^{\infty} \mu_{k\Delta} \mu_{(k+\tau)\Delta} = \frac{n-k}{n^2}.$$

Substituting this expression in equation 19, we obtain:

$$C_0 + 2 \sum_{\delta=1}^{\infty} C_{\delta} \Gamma^{\delta} = \frac{1}{n} + \frac{2}{n} \sum_{k=1}^{n-1} \left(1 - \frac{k}{n}\right) \Gamma^{k\Delta} = \frac{1}{n} + \frac{2}{n} \left(G_1 - \frac{G_2}{n}\right), \quad (21)$$

where

$$G_1 \equiv \sum_{k=1}^{n-1} \Gamma^{k\Delta}, \quad G_2 \equiv \sum_{k=1}^{n-1} k \Gamma^{k\Delta}.$$

It is not difficult then to verify that:

$$G_1 = (\mathbf{I} - \Gamma^{\Delta})^{-1} \Gamma^{\Delta} \left(\mathbf{I} - \Gamma^{(n-1)\Delta}\right),$$

$$G_2 = (\mathbf{I} - \Gamma^{\Delta})^{-2} \Gamma^{\Delta} \left(\mathbf{I} - n\Gamma^{(n-1)\Delta} + (n-1)\Gamma^{n\Delta}\right).$$

These expressions for G_1 and G_2 together with equation 19 and equation 21 fully define the covariance F for arbitrary values of λ , Δ and an arbitrary Ω .

As before, in the limit of $\Delta \rightarrow \infty$ when $\Gamma^{\Delta} \rightarrow 0$, we see that

$$F \approx \frac{S_{\lambda}}{n} \left(\mathbf{I} + \frac{2(n-1)}{n} \Gamma^{\Delta}\right) + o(\Gamma^{\Delta}).$$

In other words, as one would expect, the effective learning rate is decreased by approximately a factor of n .

A.5 Proof of Lemma 2

Proof: We have $\theta_{t_2, \lambda(t)} = \theta_{t_1} + \sum_{i=t_1}^{t_2} \lambda(i) \xi_{x_i}(\theta_i)$, where ξ_{x_i} is a stochastic gradient of batch x_i with respect to θ_i . thus

$$\frac{\theta_{t_2} + \theta_{t_1}}{2} = \theta_{t_1} + \sum_{i=t_1}^{t_2-1} \frac{\lambda(i)}{2} \xi_{x_i} \approx \theta_{t_2, \lambda(t)/2},$$

where we assumed that for fixed x_i , the gradient ξ_{x_i} changes very slowly and thus $\xi_{x_i, \lambda(t)} \approx \xi_{x_i, \lambda/2(t)}$.

Similarly for stochastic weight averaging we have

$$\theta_{\text{swa}} = \frac{1}{t_2 - t_1} \sum_{t=t_1}^{t_2} \theta_t \quad (22)$$

$$= \frac{1}{t_2 - t_1} \sum_{t=t_1}^{t_2} \left[\theta_{t_1} + \sum_{i=t_1}^{t-1} \lambda(i) \xi_{x_i} \right] \quad (23)$$

$$= \theta_{t_1} + \sum_{t=t_1}^{t_2-1} \lambda(t) \frac{t_2 - t}{t_2 - t_1} \xi_{x_t} \approx \theta_{t_2, \frac{t_2-t}{t_2-t_1} \lambda(t)} \quad (24)$$

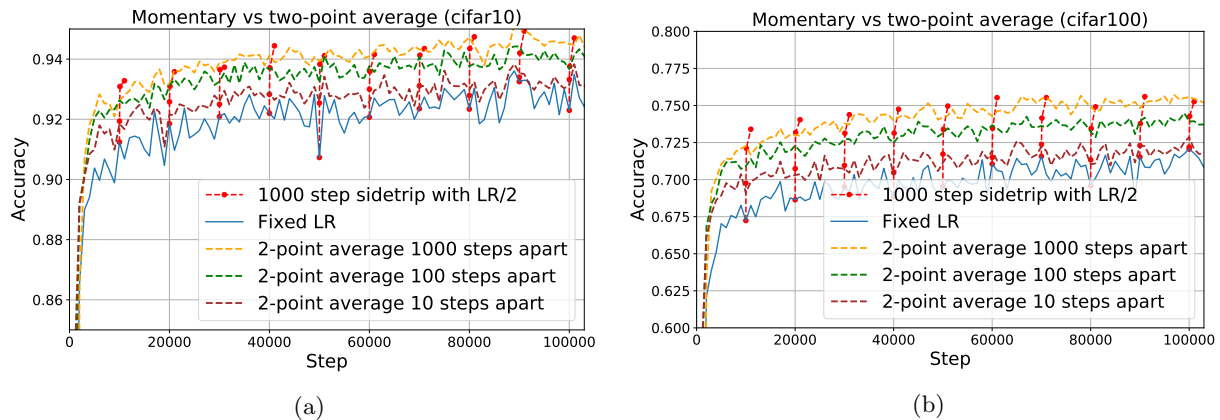


Figure 10: Two-point averaging on validation data for CIFAR10 and CIFAR100

Finally, for exponential moving average we have:

$$\theta_{\text{ema}, t_2} = \delta \sum_{t=0}^{t_2} \theta_t (1 - \delta)^{t_2 - t} \quad (25)$$

$$\approx \delta \sum_{t=t_1}^{t_2} \theta_t (1 - \delta)^{t_2 - t} \quad (26)$$

$$= \delta [\theta_{t_1} \sum_{t=t_1}^{t_2} (1 - \delta)^{t_2 - t} + \quad (27)$$

$$+ \sum_{t=t_1}^{t_2-1} \lambda(t) \xi_{x_t} \sum_{j=t}^{t_2-1} (1 - \delta)^{t_2 - j - 1}] \quad (28)$$

$$\approx \theta_{t_1} + \sum_{t=t_1}^{t_2-1} \lambda(t) (1 - (1 - \delta)^{t_2 - t}) \xi_t \quad (29)$$

where the first transition holds because we assume $t_2 - t_1 \gg 1/\delta$, and thus contribution of terms up-to t_1 is negligible. ■

B Additional Experiments

Comparison of a two-point average and an equivalent learning schedule is shown in Figure 10.

B.1 Does single-step behavior findings generalize to different batch sizes, or at different trajectory

In this section we show that our observations from the main experimental hold both at different stages of trajectory and for different batch sizes. On Appendix B.1 we show how the loss changes in a single step when

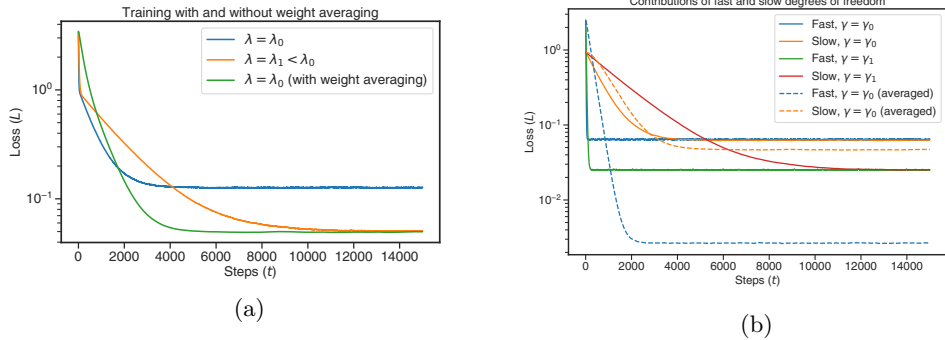


Figure 11: Loss dynamics in a system governed by with “fast” ($\Omega_{ii} = 1$) and “slow” ($\Omega_{ii} = 0.015$) degrees of freedom. (a) larger ($\lambda_0 = 5 \cdot 10^{-2}$) and smaller ($\lambda_1 = 2 \cdot 10^{-2}$) learning rates vs. Exponential Moving Average; (b) the effect of exponential moving averaging of the model weights for fast and slow degrees of freedom.

performing this step at different location of SGD trajectory and using different batch size. On Figure 13 we show the maximum loss that is achievable if we pick a step size that would pick “optimal” step. In other words the points correspond to minima of each line of Appendix B.1.

B.2 Additional experiments on Imagenet

On Appendix B.2 we show that sidetrip with appropriate learning rate schedule v.s. aggregation holds for actual loss and the accuracy, as well as for both training and test data.

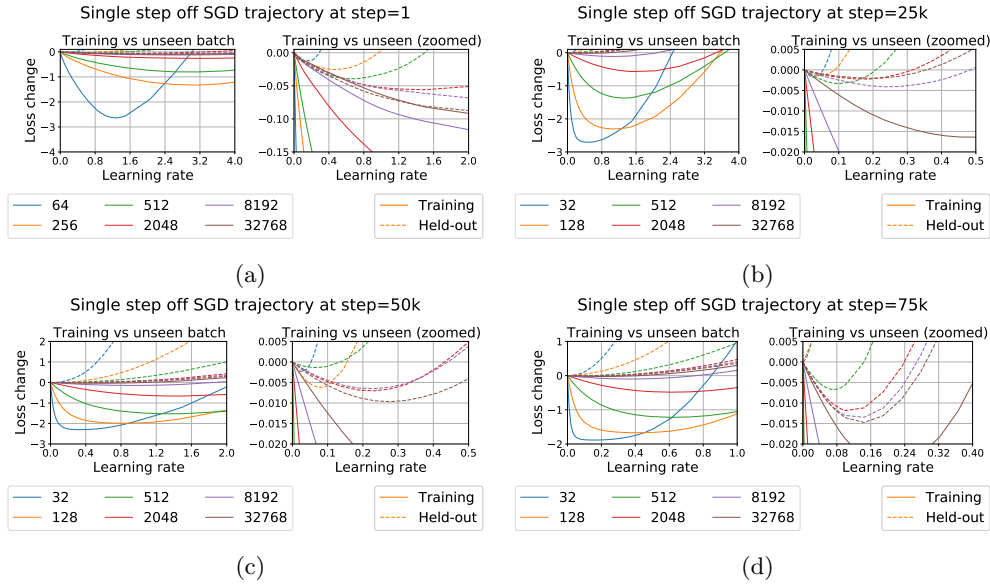


Figure 12: Loss change as a function of step size starting off different points of SGD trajectory, and using different batches.

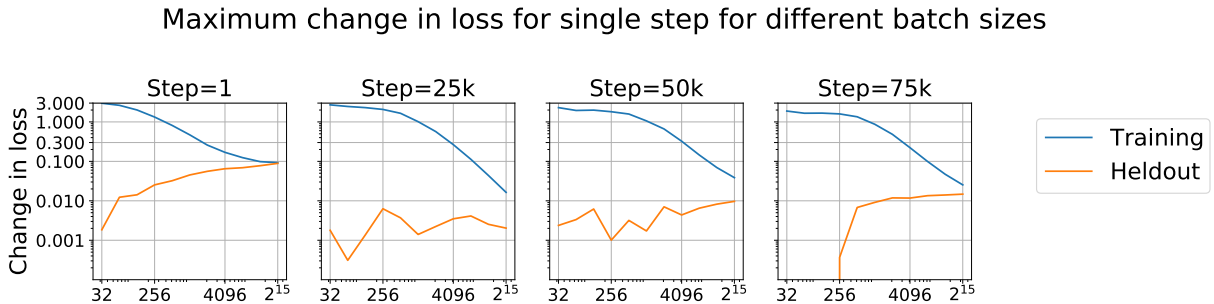


Figure 13: Maximum loss drop (log scale) for single step, when performed at different stages of SGD trajectory. As one can see even for batch size that are in the typical range (256-4096), training batch drops several orders of magnitude more than held out batch, however as the batch size reaches larger values such as 32768 the difference decreases.

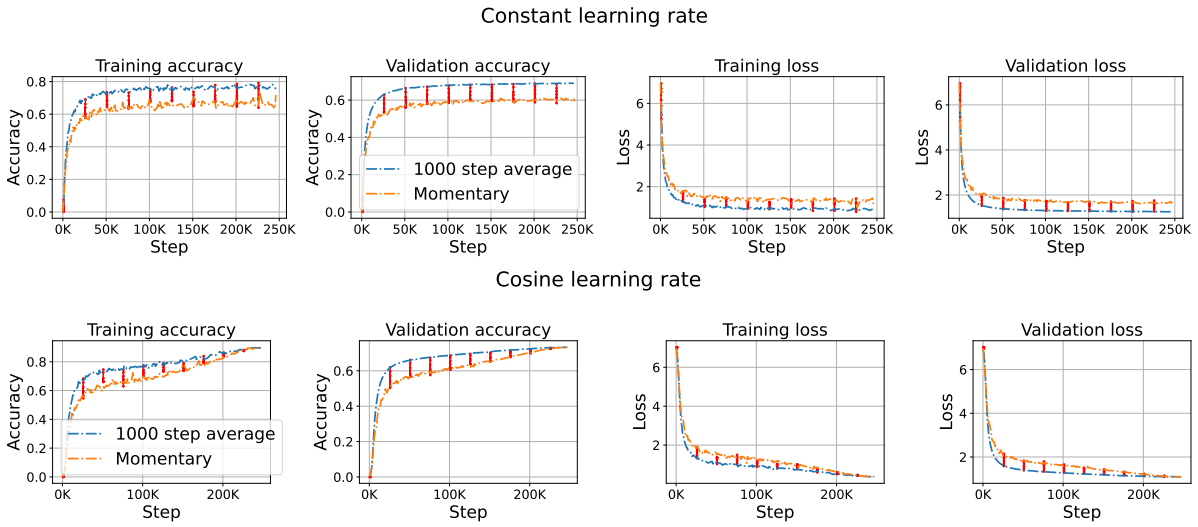


Figure 14: Accuracy and loss for training and validation splits on Imagenet. The bottom row shows the trajectory for cosine learning rate schedule, which achieves state of the art accuracy for Resnet-34 architecture. Each graph shows momentary v.s. Stochastic Averaging (SWA) and side-trips (red) with appropriate learning rate schedule.